Fano Resonance in Epsilon-Near-Zero Media

Wendi Yan,[1] Hao Li,[1,2] Xu Qin,[1] Peihang Li,[1] Pengyu Fu,[1] Kaifeng Li,[1] and Yue Li[1,3,*]
[1]Department of Electronic Engineering, Tsinghua University, Beijing 100084, China
[2]Huawei technologies co. ltd., Shanghai 201206, China
[3]Beijing National Research Center for Information Science and Technology, Beijing 100084, China

(Received 6 July 2024; revised 11 October 2024; accepted 18 November 2024; published 19 December 2024)

Fano resonance is achieved by tuning two coupled oscillators and has exceptional potential for modulating light dispersion. Here, distinct from the classical Fano resonances achieved through photonics methodologies, we introduce the Fano resonance in epsilon-near-zero (ENZ) media with novel electromagnetic properties. By adjusting the background permeability of the ENZ host, the transmission spectrum exhibits various dispersive line shapes and covers the full range of Fano parameter q morphologies, from negative to positive infinity. Furthermore, owing to the stretched electromagnetic waves in the ENZ media, ENZ Fano resonance has geometry-independent characteristics and can even be attained on a subwavelength scale. With the assistance of the Fabry-Perot mode, the background relative permeability of waveguide ENZ media can be engineered, experimentally validating the concept of ENZ Fano resonance. Our Letter has significant implications for electromagnetic metamaterials and photonic devices, with potential applications in exotic dispersion modulation and synthesis of light.

DOI: 10.1103/PhysRevLett.133.256402

Introduction—Fano resonance was discovered in 1935 [1,2] by Ugo Fano and describes the general weak coupling between a discrete localized state and a continuum of states in optics. The absorption spectrum, $\sigma(E)$, of the Fano resonance can be described by the following formula:

$$\sigma(E) = D^2(q+\Omega)^2/(1+\Omega^2), \tag{1}$$

where E is the energy, q is the Fano parameter, Ω is the normalized detuned energy, and D^2 is the normalized amplitude [3,4]. By adjusting the phase shift of the continuum oscillator, the Fano parameter q can be modified, thereby tuning the dispersive spectrum. Multiple methods [5–9] have been investigated to achieve Fano resonance. These approaches demonstrate exceptional potential for controlling light, with notable applications, including ultrasmall lasers [10], all-optical switches [11], and molecular monolayer sensors [12]. However, these methods for achieving Fano resonance typically require multiple wavelengths or free space; this leads to dimensions much larger than their wavelengths [5–7] or their restriction to a specific frequency range [8,9]. For broader applications, new Fano devices with highly flexible geometries and adjustable frequencies are urgently needed [4]. Media with extremely low permittivity, specifically epsilon-near-zero (ENZ) media, are a potential solution to this issue [13–20]. Exploiting the stretched wavelength [21], energy exchange and transmission can be attained in ENZ media with arbitrary shapes and subwavelength scales. This leads to exceptional phenomena, including supercoupling [13–18] and ideal electromagnetic (EM) flow [19,20]. By overcoming the size limitations of traditional metamaterials [22,23], typical applications have been achieved in ENZ media, such as impedance matching and cloaking [24–26], antidoping and 3D wave bending [27–29], coherent perfect absorption [30,31], ultrathin ENZ waveguides [32,33], non-Hermitian zero refractive indices [34], geometry-independent antennas [35–37], and calculus calculators [38]. Additionally, ENZ media provide an effective mechanism for weak coupling [19,20]. Thus, Fano devices can be designed with extremely small volumes and arbitrary shapes by establishing weak coupling between the ENZ media and another oscillator.

In this Letter, we introduce the Fano resonance in epsilon-near-zero media, referred to as "ENZ Fano resonance." Unlike classical Fano resonances achieved through photonics methods, this resonance is attained by establishing weak coupling between a continuum ENZ oscillator and a discrete dielectric oscillator. First, by adjusting the background relative permeability μ_h of the ENZ media, the phase shift δ of the ENZ oscillator and the Fano parameter q are effectively tuned. The dispersive spectra exhibit five distinct shapes, covering the entire range of Fano resonance morphologies. Furthermore, ENZ Fano resonance has outstanding properties, including geometry independence and an exceptionally small volume. For experimental verification, we introduce an approach to tune the background relative permeability of waveguide ENZ media assisted by the Fabry-Perot (F-P) mode [39,40], and three dispersive spectra with $q = -1$, 0, and 1 are experimentally

*Contact author: lyee@tsinghua.edu.cn

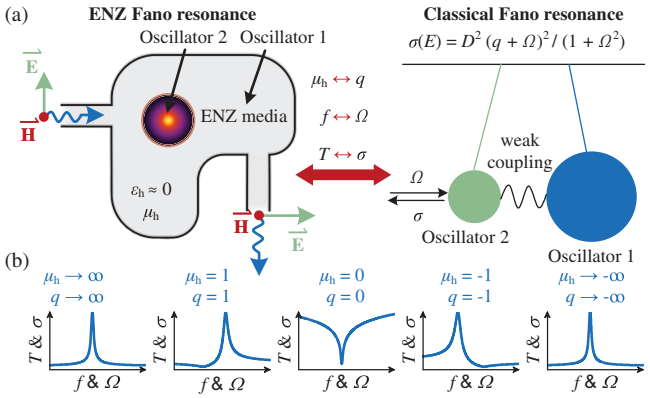

FIG. 1. Conceptual sketch of ENZ Fano resonance. (a) Correspondence between the ENZ Fano resonance and classical Fano resonance. (b) Schematic of the spectra for both ENZ and classical Fano resonances.

attained. To highlight the potential of flexible dispersive modulation in ENZ Fano resonance, sophisticated filters are engineered. ENZ Fano resonance presents significant potential for the unique modulation and synthesis of light dispersion; it has notable implications for electromagnetic metamaterials and photonic devices, spanning applications from the microwave to the midinfrared range, including lasers, all-optical switches, and on-chip photonic sensors.

General concept—To implement the concept of ENZ Fano resonance, we start by examining the conditions required to achieve the classical Fano resonance. Based on the model of two coupled driven oscillators in Fig. 1(a) [4,41], Fano resonance arises from the coupling of two oscillators with significantly different damping rates; this process leads to either narrow or broad spectral lines. Specifically, the phase of continuum oscillator 1 slowly varies, whereas discrete oscillator 2 experiences a π-phase shift at the resonant frequency [4]. By combining the resonance of the two oscillators, an asymmetrical spectral line is established; this line features a sharp transition between a dip and a peak. In addition, Fano resonance requires oscillators to operate in a weak coupling regime [42]. Once these conditions are met, the Fano formula can be used and is shown in Eq. (1). The Fano parameter q is the cotangent of δ, where δ represents the phase shift of continuum oscillator 1. q affects the morphologies of the spectral lines. Since ENZ media have demonstrated great potential to be treated as a continuum state with a weak coupling energy exchange mechanism [19,20], a discrete oscillator needs to be introduced into the ENZ media to construct ENZ Fano resonance.

Multiple types of oscillators can be introduced into ENZ media [16,32,43]. For example, we introduce a 2D dielectric oscillator to construct ENZ Fano resonance (see Supplemental Material [44] note 1). In the conceptual sketch depicted in Fig. 1, a cylindrical dielectric rod is positioned in an ENZ host. According to the Helmholtz equations [45] (see [44] note 2), the dielectric rod exhibits discrete resonant behavior at $J_0(k_d r_d) = 0$. Here, $J_0(-)$ represents the zeroth-order Bessel function of the first kind, k_d denotes the wave vector, and r_d represents the radius of the cylindrical rod. The resonance induces a sudden π phase shift, corresponding to discrete oscillator 2 in the Fano resonance. Moreover, the phase shift of continuum oscillator 1, i.e., the ENZ media, is influenced by μ_h. Consequently, as depicted in Fig. 1(b), the parameter q in ENZ Fano resonance is modulated from negative infinity to positive infinity; this results in five spectral line types that cover the entire Fano resonance morphologies.

Theoretical calculation and numerical simulation—To illustrate the geometry independence and exceptionally small volume characteristics without loss of generality, Fig. 2(a) shows an ENZ host with an irregular "cordate" shape, a relative permittivity ε_h, a relative permeability μ_h, and an area of A at a subwavelength scale. The dielectric rod, with a radius of r_d, an area of A_d, a relative permittivity ε_d, and a relative permeability $\mu_d = 1$, is positioned within the ENZ host. Two waveguides are filled with media and have normalized relative permittivity ε_p and relative permeability $\mu_p = 1$; these are used for transmitting and receiving the waves. The entire system is excited by transverse magnetic (TM) waves, with the magnetic field oriented out of plane. The Fano parameter q factor only depends on the phase shift of the ENZ host δ. The exact transmission coefficient T and reflection coefficient R of only the ENZ host can be calculated as follows [46] (see Supplemental Material [44] note 3):

$$R(\omega) = \frac{i \sin\left(\sqrt{\mu_h \varepsilon_h}\frac{\omega}{c} l\right)\left(\sqrt{\frac{\varepsilon_h}{\mu_h \varepsilon_p}} - \sqrt{\frac{\mu_h \varepsilon_p}{\varepsilon_h}}\right)}{2\cos\left(\sqrt{\mu_h \varepsilon_h}\frac{\omega}{c} l\right) - i\left(\sqrt{\frac{\mu_h \varepsilon_p}{\varepsilon_h}} + \sqrt{\frac{\varepsilon_h}{\mu_h \varepsilon_p}}\right)\sin\left(\sqrt{\mu_h \varepsilon_h}\frac{\omega}{c} l\right)}, \tag{2}$$

$$T(\omega) = \frac{2}{2\cos\left(\sqrt{\mu_h \varepsilon_h}\frac{\omega}{c} l\right) - i\left(\sqrt{\frac{\mu_h \varepsilon_p}{\varepsilon_h}} + \sqrt{\frac{\varepsilon_h}{\mu_h \varepsilon_p}}\right)\sin\left(\sqrt{\mu_h \varepsilon_h}\frac{\omega}{c} l\right)}. \tag{3}$$

Here, ω is the angular frequency, c is the speed of light in vacuum, l is the propagation length of EM waves in the ENZ media, i is the imaginary unit, and an $e^{-i\omega t}$ time convention is assumed. The Fano parameter q can be calculated using the following formula:

$$q = \cot\delta = \mathrm{cotArg}[\mathrm{R}(\omega)], \tag{4}$$

where $\mathrm{Arg}[\mathrm{R}(\omega)]$ is the phase of the reflection coefficient. Under the condition $\varepsilon_h \sim 0$, we can obtain an approximate result of the q factor, as follows:

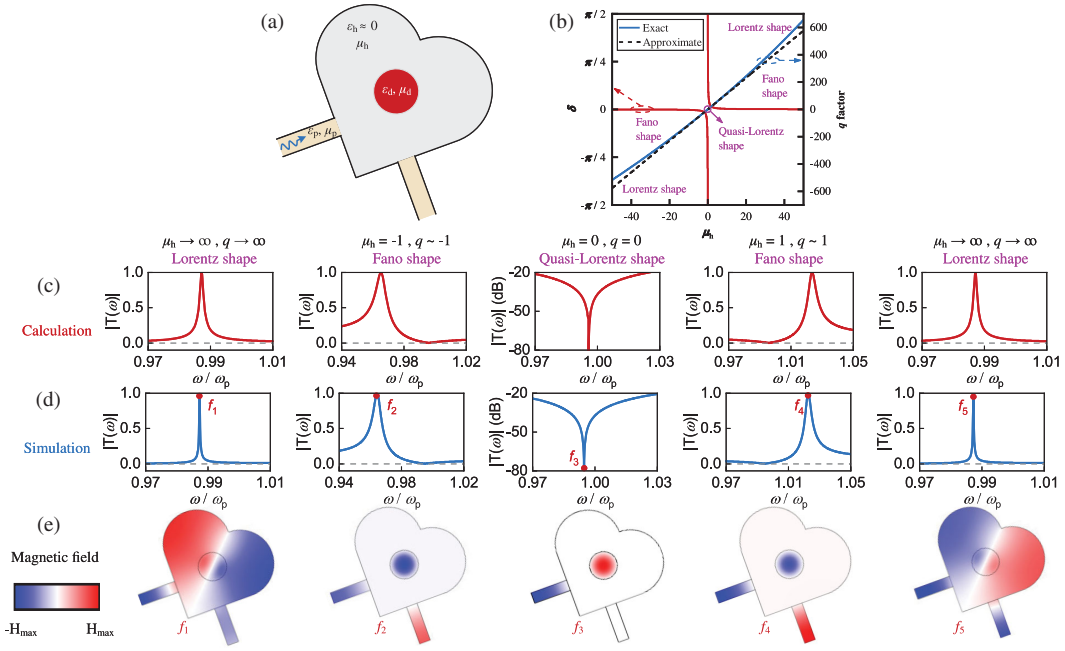

FIG. 2. Theoretical approach and numerically simulated results of ENZ Fano resonance. (a) Geometry of ENZ Fano resonance in ENZ media. (b) Relationships among the background phase shift δ, the q factor, the background relative permeability μ_h, and the linear types. (c) and (d) Theoretically calculated results and numerically simulated results of ENZ Fano resonance with different μ_h values in (a). (e) Simulated magnetic field distributions out of plane at the specialized frequencies in (d).

$$q \approx \frac{\sqrt{\varepsilon_p}\omega l}{2c}\mu_h. \tag{5}$$

To compare the numerical differences between the exact and approximate formulas, we set the specific parameters of Fig. 2(a) (see Methods in the Supplemental Material [44]). The phase shift δ, exact and approximate q factors, which change with μ_h, are presented in Fig. 2(b). The approximate results can closely match the exact results, particularly when μ_h is small. In summary, by adjusting only μ_h, we can induce changes in q to enable the full coverage of the five different morphologies and spectral line types in the ENZ Fano resonance.

To verify our predictions regarding the relationships among μ_h, q, and line types, we calculate the specified R and T of ENZ Fano resonance. We categorize them into two scenarios. First, when the μ_h and q factors are finite values (corresponding to the $q = -1$, 0, and 1 cases), the wavelength in ENZ media approaches infinity, enabling the dielectric resonance to extend across the entire ENZ media. At this time, consistent with the concept of photonic doping [19], the ENZ host together with the dielectric rod can be treated as homogeneous ENZ media with effective permeability μ_{eff} (see Supplemental Material [44] note 4):

$$\mu_{eff} = \mu_h + \frac{A_d}{A}\frac{2}{k_d r_d}\left[\frac{J_1(k_d r_d)}{J_0(k_d r_d)} - \mu_h\right], \tag{6}$$

where k_d is the wave vector in the dielectric rod and satisfies $k_d^2 = \omega^2\varepsilon_d/c^2$. Second, when both μ_h and q approach infinity, the wavelength in ENZ media reverts to finite values; thus, Eq. (6) cannot be used. An F-P mode is established, and $T(\omega)$ can be calculated according to Eq. (2). Here, l represents the propagation length and indicates the distance of the path along which electromagnetic waves propagate from one port to another (see Supplemental Material [44] note 5). From a physical perspective, when the q factor approaches infinity, the slowly changing phase distribution becomes intense, thereby breaking the weak coupling.

The area of ENZ media is set to a subwavelength size of $A_d = 0.4\lambda_p^2$ (where λ_p is the wavelength in free space), and the calculated transmission amplitudes are shown in Fig. 2(c). For comparison, simulations are provided in Fig. 2(d). When μ_h and q approach infinity, both the calculated and simulated amplitudes indicate symmetric Lorentz-shaped spectral lines. When $\mu_h = -1$ or 1, the calculated and simulated results show asymmetric Fano-shaped spectral lines. When the μ_h and q factors are equal to zero, the calculated and simulated results indicate quasi-Lorentz spectral lines. The magnetic field distributions out-of-plane at frequencies $f_1 \sim f_5$ in Fig. 2(d) are also shown in Fig. 2(e). Observations indicate that when μ_h and q approach infinity, the magnetic fields in ENZ media satisfy a half-wavelength distribution; this corresponds to the first order of the F-P mode. In contrast, in cases where $\mu_h = -1$, 0, and 1, the magnetic fields within cylindrical dielectric rods indicate Bessel modes. These behaviors align with predictions from ENZ Fano resonance [4]. In summary, by

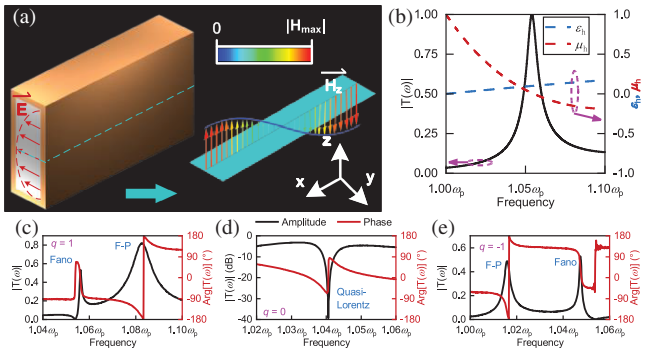

FIG. 3. Background relative permeability of waveguide ENZ media assisted by the F-P mode and experimental verification of ENZ Fano resonance. (a) 3D configuration of the F-P mode waveguide. The cross-section of the waveguide displays the equivalent transverse electromagnetic wave. The half-wavelength magnetic distribution in the z direction is also presented. (b) Changes in the calculated transmission amplitude, ε_h, and μ_h with frequency in (a). (c),(d), and (e) Experimental results of both transmission amplitudes and phases (after calibration) in the cases where $q = 1$, 0, and -1.

establishing weak coupling between the dielectric resonance and ENZ states, we achieve ENZ Fano resonance.

3D configurations—To attain ENZ Fano resonance in 3D configurations, materials with a permittivity near zero and an adjustable permeability are needed; and these material cannot be found in natural materials. One approach involves combining waveguide-emulated plasmonics [39,40] with a Drude or Lorentzian dispersive material (see Supplemental Material [44] note 6). However, the efficiency is strongly limited due to great losses in plasmonics [47]. Here, we introduce an approach to adjust the permeability in waveguide-emulated plasmonics assisted by the F-P mode.

The F-P mode is established when standing wave distributions with integer multiples of half-wavelengths are formed between two metallic boundaries along the propagation direction [48]. As illustrated in Fig. 3(a), the central cross section of the waveguide (cyan dotted line) filled with air excited by the transverse electric (TE) 10 mode possesses an actual relative permeability of $\mu_r = 1$ and a background relative permittivity as follows:

$$\varepsilon_h = 1 - c^2\pi^2/\omega^2 d^2. \tag{7}$$

The ideal ENZ frequency $\omega_p = c\pi/d$, results in ε_h equal to zero and a uniform magnetic field in the same direction. However, when ω is greater than ω_p, ε_h becomes a small positive value and causes a slow variation in the magnetic field. A half-wavelength distribution is established, as depicted in Fig. 3(a). The waveguide excited by the TE_{10} mode without a dielectric rod can be observed as background ENZ media, whose relative permeability is defined as follows [43] (see Supplemental Material [44] note 8):

$$\mu_h = \frac{2 - 2/T(\omega) - iT(\omega)(1 - c^2\pi^2/\omega^2 d^2)\omega l/(c\sqrt{\varepsilon_p})}{(1 - c^2\pi^2/\omega^2 d^2)(\omega l/c)^2 + i\sqrt{\varepsilon_p}\omega l/c}, \tag{8}$$

where l is the propagation length and ε_p is the normalized relative permittivity of the transmitting and receiving ports. The calculation of a waveguide with a length of $1.5\lambda_p$ (λ_p is the wavelength of the EM wave with ω_p in free space) is shown in Fig. 3(b). The results indicate a maximum transmission amplitude at $\omega_{F\text{-}P} = 1.052\omega_p$, with $\varepsilon_h = 0.096$ and $\mu_h = 0$. For frequencies below $\omega_{F\text{-}P}$, μ_h is positive. Conversely, when the frequency exceeds $\omega_{F\text{-}P}$, μ_h becomes negative. This proposed approach allows for an adjustable μ_h in Eq. (5) while ensuring low loss in ENZ media for the first time. Therefore, to achieve ENZ Fano resonance in this waveguide, we can adjust the propagation length of the waveguide, thereby adjusting the μ_h.

The detailed description of the experiment is provided in Supplemental Material [44] note 9. The measured transmission amplitudes and phases are shown in Figs. 3(c),3(d), and 3(e). In Fig. 3(c), the spectrum shows a Fano line type, as predicted in the $\mu_h = 1$ case. In Fig. 3(d), the spectrum provides a quasi-Lorentz line type, as predicted in the $\mu_h = 0$ case. In Fig. 3(e), the spectrum shows the other Fano line type, as predicted in the $\mu_h = -1$ case. All transmitted phase results demonstrate a π-phase shift at the dielectric resonant frequency; this shift corresponds to discrete resonance in the Fano resonance. All of the above results are consistent with the theoretical predictions. Another experiment at different frequencies is also demonstrated in Supplemental Material [44] note 10, and the results further validate the theoretical predictions. The transmission efficiency in Fig. 3 is approximately 60%; this result is attributed to strong resonance within the dielectric rod. To solve this issue, we can use an all-metallic design [37] or change the mode [16] of the dielectric rod. Additionally, we demonstrate the simulation results of ENZ Fano resonance at 100 and 400 THz in Supplemental Material [44] note 11. The results demonstrate that the devices are still functional at 100 THz. In summary, assisted by the F-P mode and waveguide-emulated plasmonics, we experimentally validate the ENZ Fano resonance in 3D configurations, and these configurations have potential applications for devices ranging from the microwave to midinfrared band.

Dispersion synthesis application—To demonstrate the potential of enabling photonic devices with dispersion modulation based on ENZ Fano resonance, two nontrivial filters with distinctive dispersive spectra are presented in this section. First, we introduce an EIT filter, whose spectrum shows a narrow bandpass (bandstop) feature in a bandstop (bandpass) filter. This filter attains narrow band filtering with frequency-selective characteristics [41,49].

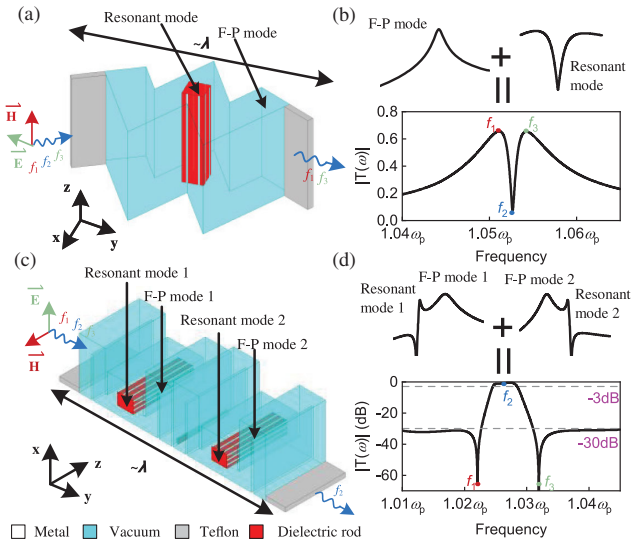

FIG. 4. Applications of dispersion synthesis assisted by Fano resonances in ENZ media. (a) 3D configuration of an electromagnetically induced transparent (EIT) filter. (b) Numerical simulation results in (a). (c) 3D configuration of a rectangular pulse filter. (d) Numerical simulation results in (b).

The configuration of the EIT filter, shown in Fig. 4(a), features an irregular shape resembling the letter "*W*" and has a volume of $0.92 \times 0.72 \times 0.5\lambda_p^3$ [see Fig. S10(a) [44]]. This design highlights the advantages of both geometric independence and subwavelength characteristics. We choose a narrower F-P mode to serve as the continuum oscillator, with a discrete oscillator. As demonstrated in Fig. 4(b), by combining these two oscillators, we obtain a simulated EIT filter with a featured spectral line; this is shown as a dip in the center of a peak. Second, we introduce a rectangular pulse filter whose spectrum demonstrates an ultranarrow bandpass filter with excellent roll-off characteristics; this filter has significant potential in communication applications [50–53]. The configuration of the rectangular pulse filter is displayed in Fig. 4(c). Assisted by the ENZ Fano resonance, we can cascade two F-P cavities modulated by dielectric rods, resulting in two F-P modes and two resonant modes. The transmission amplitude is a bandpass spectrum, as shown in Fig. 4(d) (see Fig. S11 [44] for other designs). Compared with other methods [52], the rectangular pulse filter shows nearly the best function at the subwavelength scale, highlighting the potential of applications based on ENZ Fano resonance.

Discussion—In this research, we introduce the concept of Fano resonance in ENZ media. By establishing a weak coupling between the continuum ENZ oscillator and a discrete dielectric oscillator, we achieve dispersive modulation of light. The ENZ Fano resonance has two distinct advantages. First, by adjusting the background relative permeability of ENZ media, we can reasonably adjust the Fano parameter q in various cases. Consequently, the transmission amplitude exhibits various spectral line shapes and covers the entire range of morphologies of the Fano resonances. Second, inheriting the exotic characteristics of the ENZ media, ENZ Fano resonance introduces geometry independence and subwavelength features. Thus, ENZ Fano resonance can be integrated into photonic devices. We present a theoretical framework to describe ENZ Fano resonance. Using waveguide-emulated plasmonics, we experimentally achieve adjustable permeability in ENZ waveguides, thereby validating the three dispersive spectra of ENZ Fano resonance. By exploiting the ENZ Fano resonance, flexible dispersive synthesis is attained and involves two sophisticated filters with arbitrary shapes and extremely small volumes. Our work has significant impacts on potential EM metamaterials and photonic devices, such as lasers, all-optical switches, and on-chip sensors.

Acknowledgments—Y. L. acknowledges the support from National Natural Science Foundation of China (NSFC) under Grant No. U22B2016, and the National Key Research and Development Program of China under Grant No. 2021YFA0716601.

Data availability—The simulation and experiment data that support the findings of this study are available from the corresponding author upon request.

Y. L. conceived the idea and supervised the project; W. Y. carried out the analytical derivations, full-wave simulations, and experimental verifications; H. L. and X. Q. assisted to carry out the theoretical analysis; P. L., P. F., and K. L. assisted to assemble the tested system and construct the experiment setup; all authors discussed the theoretical, numerical, and experimental aspects, together with contributing to the preparation and writing of the manuscript.

The authors declare no competing interests.

[1] U. Fano, Sullo spettro di assorbimento dei gas nobili presso il limite dello spettro d'arco, Il Nuovo Cimento (1924–1942) **12**, 154 (1935).
[2] U. Fano, Effects of configuration interaction on intensities and phase shifts, Phys. Rev. **124**, 1866 (1961).
[3] J. P. Connerade and A. M. Lane, Interacting resonances in atomic spectroscopy, Rep. Prog. Phys. **51**, 1439 (1988).
[4] M. F. Limonov, M. V. Rybin, A. N. Poddubny, and Y. S. Kivshar, Fano resonances in photonics, Nat. Photonics **11**, 543 (2017).
[5] M. V. Rybin, K. B. Samusev, I. S. Sinev, G. Semouchkin, E. Semouchkina, Y. S. Kivshar, and M. F. Limonov, Mie scattering as a cascade of Fano resonances, Opt. Express **21**, 30107 (2013).
[6] A. N. Poddubny, M. V. Rybin, M. F. Limonov, and Y. S. Kivshar, Fano interference governs wave transport in disordered systems, Nat. Commun. **3**, 914 (2012).

[7] P. Yu, T. Hu, H. Qiu, F. Ge, H. Yu, X. Jiang, and J. Yang, Fano resonances in ultracompact waveguide Fabry-Perot resonator side-coupled lossy nanobeam cavities, Appl. Phys. Lett. **103**, 091104 (2013).
[8] J. A. Fan, C. Wu, K. Bao, J. Bao, R. Bardhan, N. J. Halas, V. N. Manoharan, P. Nordlander, G. Shvets, and F. Capasso, Self-assembled plasmonic nanoparticle clusters, Science **328**, 1135 (2010).
[9] M. Y. Ilchenko, O. P. Zhivkov, R. V. Kamarali, O. V. Lutchak, O. P. Fedorchuk, O. I. V. yunov, A. G. Belous, T. O. Plutenko, and G. L. Avdeyenko, Modeling of electromagnetically induced transparency with RLC circuits and metamaterial cell, IEEE Trans. Microwave Theory Tech. **71**, 5104 (2023).
[10] Y. Yu, M. Heuck, H. Hu, W. Xue, C. Peucheret, Y. Chen, L. K. Oxenløwe, K. Yvind, and J. Mørk, Fano resonance control in a photonic crystal structure and its application to ultrafast switching, Appl. Phys. Lett. **105**, 061117 (2014).
[11] L. Stern, M. Grajower, and U. Levy, Fano resonances and all-optical switching in a resonantly coupled plasmonic–atomic system, Nat. Commun. **5**, 4865 (2014).
[12] C. Wu, A. B. Khanikaev, R. Adato, N. Arju, A. A. Yanik, H. Altug, and G. Shvets, Fano-resonant asymmetric metamaterials for ultrasensitive spectroscopy and identification of molecular monolayers, Nat. Mater. **11**, 69 (2012).
[13] M. Silveirinha and N. Engheta, Tunneling of electromagnetic energy through subwavelength channels and bends using ε-near-zero materials, Phys. Rev. Lett. **97**, 157403 (2006).
[14] B. Edwards, A. Alù, M. E. Young, M. Silveirinha, and N. Engheta, Experimental verification of epsilon-near-zero metamaterial coupling and energy squeezing using a microwave waveguide, Phys. Rev. Lett. **100**, 033903 (2008).
[15] R. Liu, Q. Cheng, T. Hand, J. J. Mock, T. J. Cui, S. A. Cummer, and D. R. Smith, Experimental demonstration of electromagnetic tunneling through an epsilon-near-zero metamaterial at microwave frequencies, Phys. Rev. Lett. **100**, 023903 (2008).
[16] W. Yan, Z. Zhou, H. Li, and Y. Li, Transmission-type photonic doping for high-efficiency epsilon-near-zero supercoupling, Nat. Commun. **14**, 6154 (2023).
[17] I. Liberal, M. Lobet, Y. Li, and N. Engheta, Near-zero-index media as electromagnetic ideal fluids, Proc. Natl. Acad. Sci. U.S.A. **117**, 24050 (2020).
[18] H. Li, Z. Zhou, W. Sun, M. Lobet, N. Engheta, I. Liberal, and Y. Li, Direct observation of ideal electromagnetic fluids, Nat. Commun. **13**, 4747 (2022).
[19] I. Liberal, A. M. Mahmoud, Y. Li, B. Edwards, and N. Engheta, Photonic doping of epsilon-near-zero media, Science **355**, 1058 (2017).
[20] Z. Zhou, H. Li, W. Sun, Y. He, I. Liberal, N. Engheta, Z. Feng, and Y. Li, Dispersion coding of ENZ media via multiple photonic dopants, Light **11**, 207 (2022).
[21] I. Liberal and N. Engheta, Near-zero refractive index photonics, Nat. Photonics **11**, 149 (2017).
[22] S. Yin, E. Galiffi, and A. Alù, Floquet metamaterials, eLight **2**, 8 (2022).
[23] L. Li, H. Zhao, C. Liu, L. Li, and T. J. Cui, Intelligent metasurfaces: Control, communication and computing, eLight **2**, 7 (2022).
[24] Z. Zhou, Y. Li, E. Nahvi, H. Li, Y. He, I. Liberal, and N. Engheta, General impedance matching via doped epsilon-near-zero media, Phys. Rev. Appl. **13**, 034005 (2020).
[25] X. Huang, Y. Lai, Z. H. Hang, H. Zheng, and C. T. Chan, Dirac cones induced by accidental degeneracy in photonic crystals and zero-refractive-index materials, Nat. Mater. **10**, 582 (2011).
[26] H. Chu, Q. Li, B. Liu, J. Luo, S. Sun, Z. H. Hang, L. Zhou, and Y. Lai, A hybrid invisibility cloak based on integration of transparent metasurfaces and zero-index materials, Light **7**, 50 (2018).
[27] C. Xu, H. Chu, J. Luo, Z. H. Hang, Y. Wu, and Y. Lai, Three-dimensional electromagnetic void space, Phys. Rev. Lett. **127**, 123902 (2021).
[28] C. Xu, G. Ma, Z. G. Chen, J. Luo, J. Shi, Y. Lai, and Y. Wu, Three-dimensional acoustic double-zero-index medium with a fourfold degenerate Dirac-like point, Phys. Rev. Lett. **124**, 074501 (2020).
[29] J. Luo, J. Li, and Y. Lai, Electromagnetic impurity-immunity induced by parity-time symmetry, Phys. Rev. X **8**, 031035 (2018).
[30] J. Luo, B. Liu, Z. H. Hang, and Y. Lai, Coherent perfect absorption via photonic doping of zero-index media, Laser Photonics Rev. **12**, 1800001 (2018).
[31] D. Yan, R. Mei, M. Li, Z. Ma, Z. H. Hang, and J. Luo, Controlling coherent perfect absorption via long-range connectivity of defects in three-dimensional zero-index media, Nanophotonics **12**, 4195 (2023).
[32] Z. Zhou, Y. Li, H. Li, W. Sun, I. Liberal, and N. Engheta, Substrate-integrated photonic doping for near-zero-index devices, Nat. Commun. **10**, 4132 (2019).
[33] W. Ji, J. Luo, H. Chu, X. Zhou, X. Meng, R. Peng, M. Wang, and Y. Lai, Crosstalk prohibition at the deep-subwavelength scale by epsilon-near-zero claddings, Nanophotonics **12**, 2007 (2023).
[34] L. Luo, Y. Shao, J. Li, R. Fan, R. Peng, M. Wang, J. Luo, and Y. Lai, Non-Hermitian effective medium theory and complex Dirac-like cones, Opt. Express **29**, 14345 (2021).
[35] H. Li, Z. Zhou, Y. He, W. Sun, Y. Li, I. Liberal, and N. Engheta, Geometry-independent antenna based on Epsilon-near-zero medium, Nat. Commun. **13**, 3568 (2022).
[36] Y. Zhang, Y. Li, W. Zhang, Z. Zhang, and Z. Feng, Omnidirectional antenna diversity system for high-speed onboard communication, Engineering **11**, 72 (2022).
[37] Y. Zhang and Y. Li, Wideband microstrip antenna in small volume without using fundamental mode, Electromagn. Sci. **1**, 1 (2023).
[38] H. Li, P. Fu, Z. Zhou, W. Sun, Y. Li, J. Wu, and Q. Dai, Performing calculus with epsilon-near-zero metamaterials, Sci. Adv. **8**, eabq6198 (2022).
[39] W. Rotman, Plasma simulation by artificial dielectrics and parallel-plate media, IRE Trans. Antennas Propag. **10**, 82 (1962).
[40] Y. Li, I. Liberal, and N. Engheta, Structural dispersion based reduction of loss in epsilon-near-zero and surface plasmon polariton waves, Sci. Adv. **5**, eaav3764 (2019).
[41] Y. Yang, I. I. Kravchenko, D. P. Briggs, and J. Valentine, All-dielectric metasurface analogue of electromagnetically induced transparency, Nat. Commun. **5**, 5753 (2014).

[42] G. Khitrova, H. M. Gibbs, M. Kira, S. W. Koch, and A. Scherer, Vacuum Rabi splitting in semiconductors, Nat. Phys. **2**, 81 (2006).
[43] W. Yan, Z. Zhou, H. Li, W. Sun, Q. Lv, and Y. Li, Low-loss epsilon-near-zero metamaterials, Laser Photonics Rev. **17**, 2201000 (2023).
[44] See Supplemental Material at http://link.aps.org/supplemental/10.1103/PhysRevLett.133.256402 for information on materials and methods, for detailed derivation of formulas, for detailed description of experiments, and for additional simulations.
[45] J. D. Jackson and R. F. Fox, Classical electrodynamics, 3rd ed., Am. J. Phys. **67**, 841 (1999).
[46] D. M. Pozar, *Microwave Engineering* (John Wiley & Sons, New York, 2011).
[47] D. Korobkin, Y. Urzhumov, and G. Shvets, Enhanced near-field resolution in midinfrared using metamaterials, J. Opt. Soc. Am. B **23**, 468 (2006).
[48] X. Qin and Y. Li, Superposition of ε-near-zero and Fabry-Perot transmission modes, Phys. Rev. Appl. **16**, 024033 (2021).
[49] B. Peng, Ş. K. Özdemir, W. Chen, F. Nori, and L. Yang, What is and what is not electromagnetically induced transparency in whispering-gallery microcavities, Nat. Commun. **5**, 5082 (2014).
[50] H. Rohling, *OFDM: Concepts for Future Communication Systems* (Springer Science & Business Media, Berlin, 2011).
[51] S. Khani, M. Danaie, and P. Rezaei, Realization of single-mode plasmonic bandpass filters using improved nanodisk resonators, Opt. Commun. **420**, 147 (2018).
[52] Y. Ding, M. Pu, L. Liu, J. Xu, C. Peucheret, X. Zhang, D. Huang, and H. Ou, Bandwidth and wavelength-tunable optical bandpass filter based on silicon microring-MZI structure, Opt. Express **19**, 6462 (2011).
[53] D. Pan, B. You, X. Wen, and X. Li, Wideband substrate integrated waveguide chip filter using spoof surface plasmon polariton, Micromachines **13**, 1195 (2022).